

Review

# From Transparent Cranial Windows to Multifunctional Smart Cranial Platforms

Nana Yang <sup>1,2</sup>, Qing Li <sup>1,3,\*</sup>, Xinyue Zhang <sup>1,3</sup>, Jingjing Xu <sup>4</sup> , Shengyong Xu <sup>2</sup>  and Fengyu Liu <sup>5,\*</sup>

- <sup>1</sup> Center of Digital Dentistry, Peking University School and Hospital of Stomatology, Beijing 100081, China  
<sup>2</sup> Key Laboratory for the Physics & Chemistry of Nanodevices, School of Electronics, Peking University, Beijing 100871, China  
<sup>3</sup> National Engineering Laboratory for Digital and Material Technology of Stomatology, Beijing 100081, China  
<sup>4</sup> School of Microelectronics, Shandong University, Jinan 250100, China  
<sup>5</sup> Neuroscience Research Institute, Department of Neurobiology, Key Laboratory for Neuroscience, School of Basic Medical Sciences, Ministry of Education/National Health Commission, Peking University, Beijing 100191, China  
\* Correspondence: qingli@bjmu.edu.cn (Q.L.); liufyu@bjmu.edu.cn (F.L.)

**Abstract:** In this paper, we briefly reviewed the development of cranial windows and their functions in brain sciences. We demonstrated that a 3D-printed titanium frame coated with a polydimethylsiloxane (PDMS) film could serve as an excellent transparent cranial window for long-period, in vivo optical experiments in mice and rats, and the devices also allowed multiple injections through the elastic PDMS window, without leaking. Our large-area honeycomb structured Ti-PDMS samples had a relative transparent area ratio of over 90% but a mechanical strength close to that of a human skull, showing a promising potential for applications in large animals as multifunctional cranial windows. We also suggested that more functional modules could be integrated in the large-area Ti-PDMS cranial device, thus turning it into a novel wearable smart platform for wireless data communication, electro-probing and brain stimulation, optical imaging, transcranial injection, and so on, for both fundamental research on neuroscience and clinical practices dealing with brain damage and disease.

**Keywords:** transparent cranial window; bio-compatibility; 3D printing; titanium alloy; in vivo optical imaging; transcranial injection; wearable electronic device



**Citation:** Yang, N.; Li, Q.; Zhang, X.; Xu, J.; Xu, S.; Liu, F. From Transparent Cranial Windows to Multifunctional Smart Cranial Platforms. *Electronics* **2022**, *11*, 2559. <https://doi.org/10.3390/electronics11162559>

Academic Editor: Han Eol Lee

Received: 9 July 2022

Accepted: 8 August 2022

Published: 16 August 2022

**Publisher's Note:** MDPI stays neutral with regard to jurisdictional claims in published maps and institutional affiliations.



**Copyright:** © 2022 by the authors. Licensee MDPI, Basel, Switzerland. This article is an open access article distributed under the terms and conditions of the Creative Commons Attribution (CC BY) license (<https://creativecommons.org/licenses/by/4.0/>).

## 1. Role of Cranial Window in Brain Research

The human brain is a very complicated organ. It works in a “black box” skull, where it obtains external information through bundles of neuron axons that connect to body sensors for light, sound, smell, taste, touch, gravity, temperature, etc. The decisions of the brain are also transported out through neuron axons and turn into body actions or inner organ reactions. Most details of the working mechanisms of a brain, such as “How Are Memories Stored and Retrieved?”, remain unknown to date [1–5].

A brain consists of numerous neurons, axons, glial cells, blood vessels, water, and macromolecules, such as protein, a variety of ions with proper concentrations, etc. [6–14]. In the last century, a number of noncontact, whole-brain imaging technologies were developed, including computed tomography (CT) [15,16], magnetoencephalography (MEG) [17,18], positron emission computed tomography (PET) [19,20], functional magnetic resonance imaging (fMRI) [21,22], etc. Among them, PET is applied to monitor the 3D intensity of metabolism status in different regions of a live brain, while fMRI could present the correlation between structure and function at different parts of a live brain down to a spatial resolution of 0.1 mm.

On the other hand, contact probes with various neural electrodes have also been well-developed. By using an external electrode array attached to a head surface, electroencephalogram (EEG) technique measures and records the electrical signals of a whole

brain. Preliminary results showed that by decoding the recorded signals, a computer might roughly understand an idea running inside the brain [23].

Other kinds of electrodes were designed for implantation at the cortex surface, inside a shallow layer of the cortex, or deeply into a brain [24]. These electrodes were used to probe the excitation status of individual neurons or electrical pulses of axons and dendrites to reveal the working mechanisms for body motion, sensing, pain, decision making, etc. [25–32]. Some deep brain stimulation (DBS) electrodes have already been applied in clinical therapy [33–35].

Cranial windows offer a unique approach for brain studies: they open a transparent window on a “black box” skull for direct observation of a live brain and optical imaging of brain tissues and individual neurons [36]. With the help of high-quality cranial windows, two-photon imaging, optogenetics, confocal imaging, optical stimulation technique etc., were applied to perform in vivo optical studies of live animals, and numerous exciting results were obtained [37–47]. Multi-modular studies using combined electrical and optical techniques as well as whole brain imaging techniques led to a better understanding of brain function in complicated animal behaviors [48–62]. In some studies, injection of drugs was applied to regulate brain functions [63–73] for which a cranial window could also play an important role as a transcranial interface.

In this paper we briefly review the development of cranial windows. We describe a novel hybrid cranial device with a 3D-printed titanium alloy (Ti, Ti6Al4V) net-shaped frame combined with a transparent polydimethylsiloxane (PDMS) window, which is suitable for long-period, in vivo optical experiments in mice and rats, and allows transcranial injection without leaking. We will show that large-area honeycomb structured Ti-PDMS samples are good candidates for multifunctional cranial windows in large animals, and they can be further developed into an integrated smart device on the head.

## 2. Development of Cranial Windows

Basically, a cranial window opens a transparent window on the “dark-box” skull for direct optical observation of brain tissues and related optical experiments [36,45,61,74–76]. The glass cranial window technique was firstly attempted in the 1850s [77,78]. In the next half century, cranial windows have been developed in many different groups [36,79–82]. In the following, we will briefly introduce several cranial windows for optical observation and multifunctional cranial windows that allow optical and electrical measurements or drug delivery.

### 2.1. Natural Cranial Windows

Natural cranial windows mainly help on-site observation of brain tissues and blood vessels and in vivo optical imaging experiments. They do not require craniotomy operation and thus ensure less risk of surgery bleeding, post-operative hematoma, and inflammation.

One kind of natural cranial window was made with mechanical thinning and polishing techniques on a mouse skull [83,84]. At a target location, a small piece of the skull bone was thinned to 15–30  $\mu\text{m}$  and polished, and it turned into transparent status for studying the blood velocity in vessels [85], optical imaging of cell morphology [83,86,87], and status of neural dendrites [83,88–91]. However, this technique was only applicable to a small area of 0.1–0.3  $\text{mm}^2$  in small animals, such as mice [83,91–93], and bond cells and tissues always regrew a few days after the thinning operation. In some cases, to repeat the same thinning operation, a waiting period of as long as 18 months or longer was needed [36,83,89,94].

Recently, another kind natural cranial window was to turn a whole skull of a mouse into a transparent one by using bio-chemical techniques. Progresses were made to improve the transparency and observable depth of brain tissues [95–103].

### 2.2. Implanted Optical Cranial Windows

Implanted cranial windows were usually made of thin glass sheets or transparent polymer sheets as the window material. First the target region of an animal was undergone

a craniotomy operation, then a transparent window was implanted to replace a small part of the skull. The edge of the device was then sealed and fixed with the remaining bond by using a bio-compatible glue such as dental cement [104–106]. For general studies, the cranial window was built directly on the dura matter [58,107–118]. However, for high-resolution optical imaging or applications in large animals, the dura matter was usually removed before implantation [75,119–124]. As normal glass sheets were flat and might cause additional pressure against the brain tissues, a curved crystal window was developed, which ensured a continuous optical imaging of millions of neurons for a long period from weeks to a whole year [45,125,126].

Instead of using plain or curved glass, researchers also applied lenses in novel implanted cranial windows [127–133]. By using these novel devices, for instance, two-photon imaging was performed for neurons located as deep as 5 mm under the brain surface [131].

Polymer windows were developed in recent years from PDMS [74,76,134], polyethylene terephthalate [61], PMMA-Plexiglas [135], silicone glue gel [136], and so on. In addition to excellent optical properties, elastic polymer windows could allow penetration of a needle and had a useful self-sealing nature, thus leading to an on-site injection function [74,134].

However, the cranial windows described above were mainly developed for observation with human eyes and for optical imaging experiments. The increasing demands of neuroscience have promoted developments of multifunctional cranial windows, which allowed two or three different functions performed simultaneously.

### 2.3. Multifunctional Cranial Windows

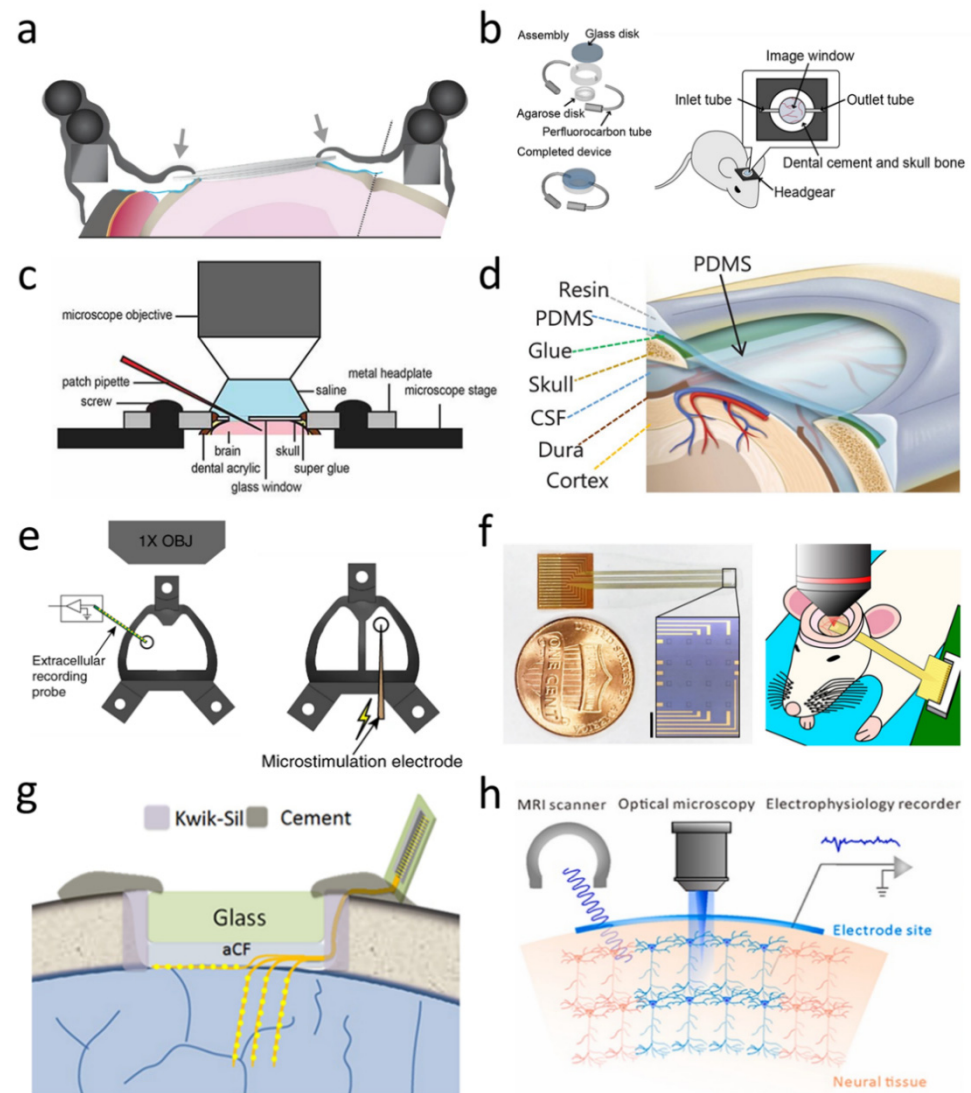
Over the years, many kinds of multifunctional cranial windows have been developed. Here, we briefly introduce some of them.

Figure 1a schematically illustrates a cross-section view of a chronic cranial window suitable for implantation in a live mouse, where its transparent window is made of a glass sheet [65]. Impressively, this piece of glass window was designed to be removable, adjustable in position, and could be replaced after weeks and months. It allowed *in vivo* experiments over several months, such as two-photon imaging of targeted region with an attached micropipette. By removal of the window, it allowed micro-surgery such as injections and cutting away overgrown tissues [65].

Figure 1b presents an idea of “lab-on-a-brain” on a mouse, where a micro-optical fluidic device is built in a cranial window [67]. The transparent micro-optical fluidic device enabled long-term *in vivo* imaging of neurons, as well as delivery of chemicals into brain tissues with low tissue damage. By using this device, the formation and elimination of spines on particular dendrite location was recorded for weeks, and spine shrinkage after two-photon uncaging stimulation was observed *in vivo*.

Figure 1c shows the structure of another kind of cranial window for mice, where it consists of a glass coverslip, and a small hole with a silicone seal was pre-made on the glass coverslip [64]. Thus, it was capable of self-sealing after multiple injections or retraction of a pipette, an electrode through the silicone seal. Over a period of 7 weeks, repeated injection experiments were performed without causing any infections of the brain.

Figure 1d illustrates a 3D structure of a transparent PDMS cranial window for rats and mice [74]. The PDMS sheet was flexible, penetrable, and elastic. It was glued to the skull with a cyanoacrylate adhesive and sealed with a dental resin. After implantation of the PDMS cranial window, *in vivo* hemodynamic responses were continuously monitored in cortical vasculatures up to 15 weeks. Insertion of microelectrodes and micropipettes into the cortical tissue through the PDMS window were performed without causing any fluid leakage. Longitudinal two-photon microscopic images of mice were also obtained in similar quality to that using glass cranial window. Interestingly, no obvious adhesion of cell or tissue on the PDMS window was monitored during the long-term observations.



**Figure 1.** Eight kinds of typical multifunctional cranial windows in brain studies. (a) A cross-section view of a chronic cranial window where the glass sheet could be replaced. Adapted with permission from [65]. 2014, Springer Nature. (b) “Lab-on-a-brain” on a mouse. Adapted with permission from [67]. 2014, Hiroaki Takehara et al. (c) A glass cranial window with a built-in silicone sealed hole for multiple injections. Adapted with permission from [64]. 2014, Christopher J. Roome and Bernd Kuhn. (d) A PDMS cranial window for rats and mice. Adapted with permission from [74]. 2016, Chaejeong Heo et al. (e) A “See-Shells” cranial window for combined electrical and optical experiments. Adapted with permission from [61]. 2019, Leila Ghanbari et al. (f) A transparent graphene sheet was applied as microelectrodes under a glass coverslip. Adapted with permission from [137]. 2018, Martin Thunemann et al. (g) Ultra-flexible nano-electronic threads was applied as microelectrodes under a glass cranial window. Adapted with permission from [50]. 2018, Elsevier. (h) A cranial window with “hydrogel-elastomer neural interface”. Adapted with permission from [62]. 2022, Elsevier.

Figure 1e is a top-view of a so-called “See-Shells” cranial window [61]. It was a large-area, transparent polymer skulls designed for a long-term optical observation of mouse cortex over 10 months. It allowed two-photon imaging of neural structures up to 600  $\mu\text{m}$  deep at a subcellular resolution and calcium imaging from multiple regions. It also had a potential to combine electrical and optical functions, i.e., to perform neural probing for electrical activities and whole cortex imaging at the same time.

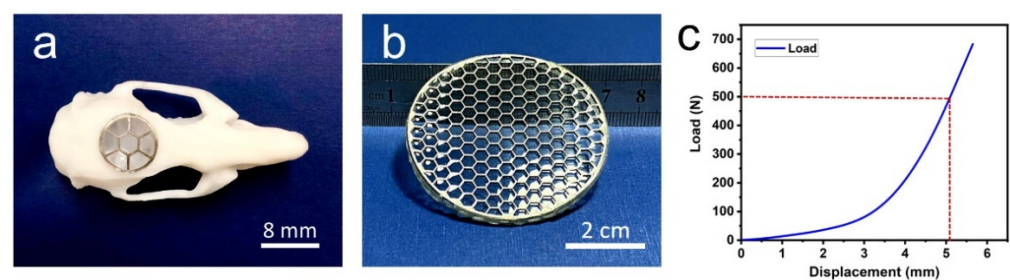
Early attempts for fabrication metallic electrodes on transparent cranial windows faced problems in combined optical and electrical measurements [57,138]. A bunch of novel electrode materials, such as graphene [55], flexible nano-electronic threads [56], carbon nanotube films [60], and organic transistor [139,140] were investigated to serve as transparent electrodes on cranial windows. As shown in Figure 1f, a transparent graphene sheet was applied as a microelectrode under a glass coverslip [137]. It allowed integration of in vivo two-photon imaging, optogenetic stimulation, and cortical recordings in one experiment [58,59,137]. In Figure 1g, arrays of ultra-flexible nano-electronic threads were implanted in a mouse for neural recording both at the brain surface and deep-level locations, then a glass sheet cranial window was sealed on the top [50]. This multimodal platform allowed a combination experiment for both laser speckle contrast imaging of cerebral blood flow and electrical recording of neural activity at particular positions [50,56,58].

Figure 1h demonstrates the main concept of a novel cranial window named as “hydrogel-elastomer neural interface”. This unique window allowed multifunctional experiments of electrophysiology, optical microscopy such as two-photon imaging, as well as magnetic resonance imaging [62]. The hydrogel and elastomer showed comparable elastic moduli to neural tissues and dura mater and could fit well to the curved brain surface. Simultaneous electrical recording and optical imaging were performed, and in MRI experiments the soft interface did not cause artifact images.

Nevertheless, the above transparent cranial windows do not seem suitable for large animals. Glass sheets are hard but fragile and easy to break. PDMS sheets are too soft to protect the brain tissue from external strikes. In the following, we present an alternative approach for large-area, transparent cranial window with superior mechanical strength made of Ti frames.

### 3. A Hybrid Ti-PDMS Structure for Large-Area Transparent Cranial Window

Three dimensional (3D) printing is now a well-developed technology [141–144]. By using laser scanning technique and 3D printing technique, we can fabricate complicated 3D structures with shape, thickness and curvature matching exactly to the designed dimensions from a variety of materials, such as resin, plastic and metal. For example, Figure 2a is a 3D printed resin sample, following the same shape of a rat skull sample [63]. The circular subject fit in the top surface of this resin skull was a Ti cranial window.



**Figure 2.** (a) A resin rat skull sample made by 3D printing technique with resin. In the middle of the top surface, a curved, 3D-printed circular Ti cranial window was fitted. Adapted with permission from Ref. [63]. 2022, Nana Yang et al. (b) Optical photograph of a 50 mm diameter, net-like Ti-PDMS cranial window. The circular Ti frame with thin hexagonal grids was firstly 3D-printed, polished, and then covered with a PDMS layer. (c) Raw data of mechanical test for one 50 mm diameter Ti-PDMS cranial window. It needed a static force of 500 N perpendicular to the Ti-frame at the center to let the central region show a 5 mm displacement.

Ti was chosen as the basic material for our cranial windows. Ti is metal with superior properties and has been extensively used in medial and clinical applications [145–151]. Figure 2b is an optical photograph of a honeycomb structured Ti-PDMS cranial window. Made by 3D printing technique, the circular Ti frame had a diameter of 50 mm. Within the circular frame were uniform hexagonal Ti grids, each grid had a thickness of 0.3 mm and

height of 1.0 mm. By using this thin grid structure, we obtained the ratio of the opening area to the total device area as high as  $90 \pm 7\%$ , depending on the grid size. After 3D-printed, the Ti frame was mechanically polished, then put in a homemade mould to cover a thin layer of PDMS.

The honeycomb structure has been well studied and applied [152–157]. Our honeycomb structured Ti cranial windows weighed only 6–7 g, yet they had a remarkable mechanical strength. Figure 2c presents a typical raw data taken from mechanical test for a 50 mm diameter Ti-PDMS cranial window. During the test, a stainless-steel rod of 15 mm in diameter was pushed slowly and perpendicularly to the Ti-frame surface at the center. To cause the central region a displacement of 5 mm, it required a static force of 400–500 N [63]. This mechanical strength was close to that of a human skull [158]. If such a Ti frame was implanted as a cranial window on a large animal, it should be able to protect the brain from external strikes.

Note that this Ti grid has a thickness of only 1.0 mm. For application in human skulls, one can increase the thickness to 2–3 mm, thus making the Ti-grid cranial window much stronger. Also, as Ti is a nonmagnetic material, Ti cranial window is compatible to MRI and CT imaging [146].

For the transparent window, PDMS was chosen in our device. PDMS is an elastic transparent polymer and has perfect compatibility to bio-tissues [159–164]. As reviewed in this paper, PDMS has been applied in transparent cranial windows [74,134]. PDMS is a hydrophobic material. Figure 3 presents a typical set of results in contact angle measurements with saline water and PBS solution for our PDMS samples and glass cover slides. It showed that the contact angles for PDMS were approximately  $109^\circ$  for saline water and around  $106^\circ$  for PBS solution. In contrast, for glass cover slides these angles were approximately  $37^\circ$  and  $52^\circ$ , respectively. The hydrophobic nature of PDMS helped a lot in our Ti-PDMS cranial windows, which avoided obvious growth of cells or adhesion of bio-materials on the inner side of these PDMS windows, when they were implanted in live animals. For instance, our experiments showed that after implantation in mice for 140 days, the Ti-PDMS hybrid window retained almost the similar clearness as that of Day 1, and the microstructural details of brain blood vessels were clearly recorded from outside [63].

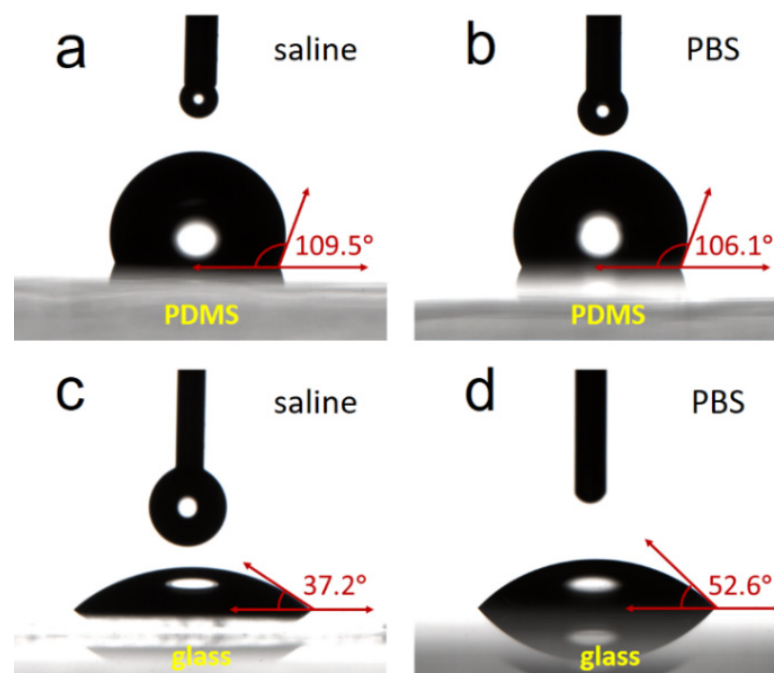


**Figure 3.** Contact angle measurements for PDMS and glass cover slide. (a) Saline on PDMS. (b) PBS on PDMS. (c) Saline on glass slide. (d) PBS on glass slide.

When coating the polished Ti honeycomb frame with PDMS, some small bubbles were likely to remain in the as-made PDMS windows, as shown in Figure 4a. We have developed a multistage process, where the samples were continuously shaken and degassed with certain equipment, and clear Ti-PDMS samples were obtained without noticeable bubbles, as shown in Figure 4b.

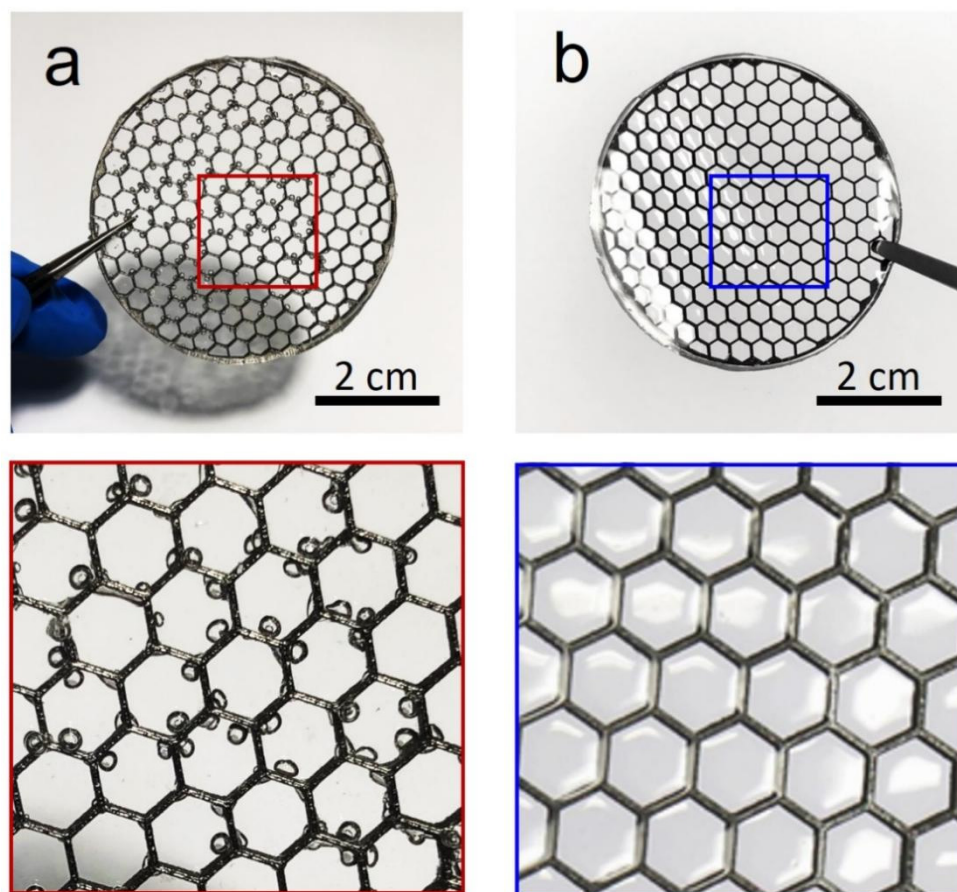


**Figure 4.** Photographs for Ti-PDMS cranial window samples. (a) Simple dipping process of the Ti frame in PDMS caused micro-bubbles. (b) By using a multistage shaking and degassing processes, the gas bubbles were totally removed from the sample.

In the wavelength range of 380–1100 nm, PDMS layer (0.3–0.5 mm in thickness) showed a higher transmittance than that of #1 glass coverslip. Therefore, our small-size Ti-PDMS transparent cranial windows implanted in mice allowed excellent two-photon imaging results [63]. The excellent plastic nature of PDMS was utilized to perform multiple injection of drugs using commercial 1 mL syringe through the same unit window of PDMS on a honeycomb Ti frame. For continuous injections by 15 times, no leaking of the injected liquid was observed. Figure 5 showed a typical result after injection of DiI (0.1% methanol in water, 0.2  $\mu\text{L}$ , 0.1  $\mu\text{L min}^{-1}$ ) and fluorescence dye CTB488 (1 mg  $\text{ml}^{-1}$  in PBS, 0.2  $\mu\text{L}$ , 0.1  $\mu\text{L min}^{-1}$ ) at three different spots of a mouse cortex through an implanted Ti-PDMS cranial window. No leaking was observed after the injections. Two days later, confocal imaging experiments were performed at the injection region. As shown in Figure 5d, the three injection spots were clearly observable, and fluorescence dye was recorded in deeper tissues around the injection spot [63].

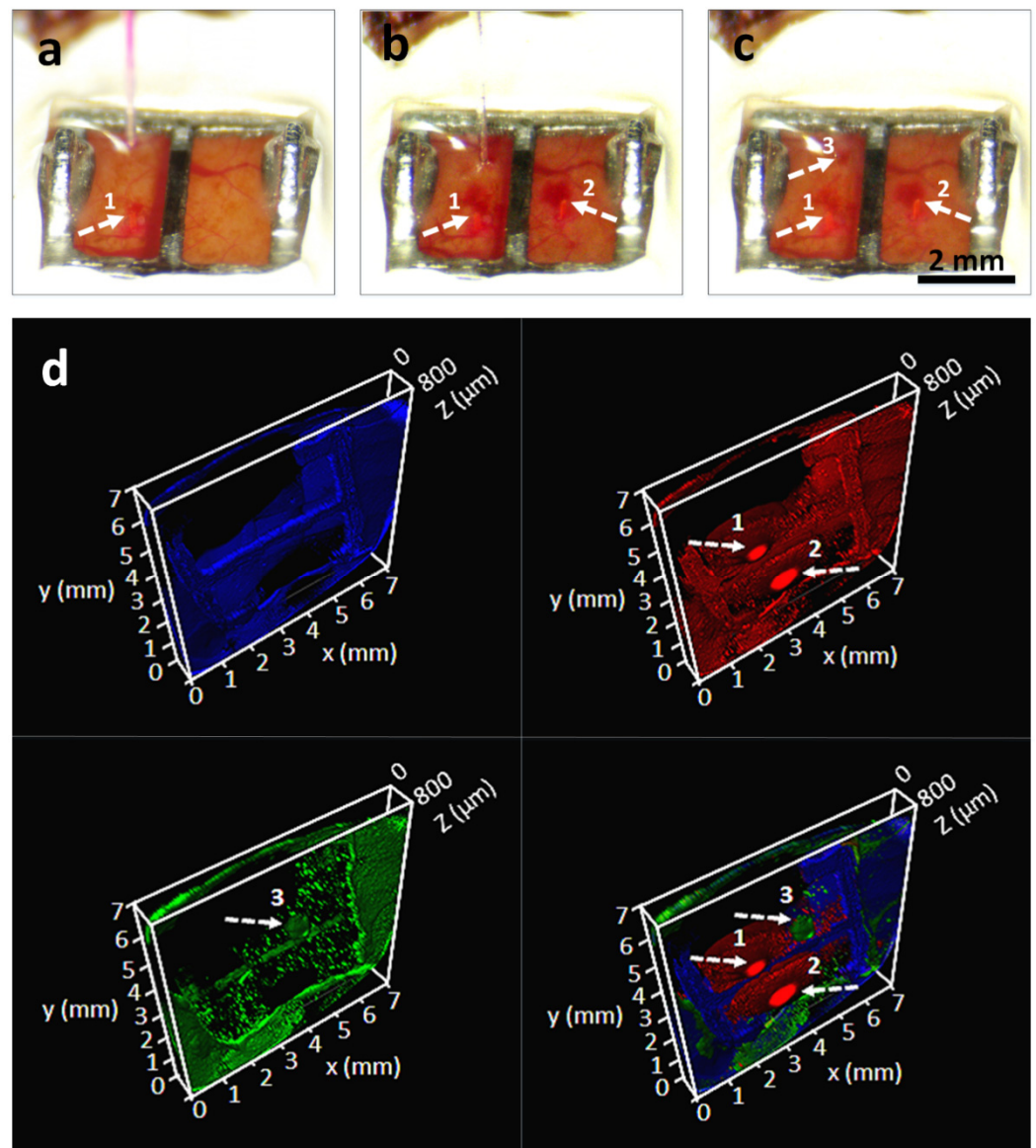


**Figure 5.** (a–c) Photographs for injections of DiI at spots 1 and 2 ( $0.1\%$  in methanol,  $0.2 \mu\text{L}$ ,  $0.1 \mu\text{L min}^{-1}$ ) and fluorescence dye CTB488 ( $1 \text{ mg mL}^{-1}$  in PBS,  $0.2 \mu\text{L}$ ,  $0.1 \mu\text{L min}^{-1}$ ) at spot 3 through a Ti-PDMS cranial window implanted on a mouse head. (d) Confocal imaging micrographs for the injected spots after two days. Adapted with permission from [63]. 2022, Nana Yang et al.

#### 4. Discussion

Our small size Ti-PDMS cranial windows worked well in rats and mice for optical experiments and drug injections. Our preliminary results have shown that Ti-PDMS cranial windows could be implanted in live animals for 5 months without causing any observable inflammation of brain tissues or other side effects [63].

Aiming at potential applications as large-area transparent cranial windows, our 3D-printed honeycomb-structured Ti frames showed excellent mechanical strength against external strikes. Weighing only approximately 7 g, the 50 mm diameter, 1 mm thick honeycomb-structured Ti frame presented a displacement of 5 mm at the center under an external static force of 400–500 N. On the other hand, the 3D printing technique used in this work allowed personal designs for special size, curvature, thickness, and transparent ratio in various applications on different animal skulls [63].

The excellent transparent properties of PDMS in a hybrid Ti-PDMS cranial window offered an ideal optical window for long-period, real-time observation of brain status or

to perform a variety of *in vivo* optical experiments such as two-photon imaging, confocal imaging, optogenetics, etc. [63,74].

The good elastic nature of the PDMS window also allowed multiple impaling of injectors for injection of drugs into the brain or extraction of hydrocephalus from the brain, without leaking. This merit was quite valuable in both brain studies and clinic applications [63,74]. For example, it could be applied to perform drug delivery bypassing the blood–brain barrier.

Finally, the non-magnetic nature of both Ti and PDMS also made the Ti-PDMS devices compatible to CT and MRI measurements.

The above merits made the hybrid Ti-PDMS device a promising candidate for implantation in big animals as a large-area, transparent, high-strength, multifunctional cranial window.

Indeed, such a multifunctional cranial window may lead to a wearable, smart electronic device for both medical and health care applications. Recent developments of microchips, 5G wireless communication technology, and neural probing techniques make this proposal practical.

For instance, Neuralink Co. has demonstrated that a brain–computer interface mounted in the skull of a pig or a monkey, with the size of a quarter coin, and consisting of built-in processing chips, circuits and battery, could collect the real-time neural signals of the animal through thousands of microelectrodes implanted in the brain cortex [165]. This could be considered as a simple prototype of a smart cranial electronic device.

As illustrated in Figure 6, a complicated smart cranial electronic device, once developed, may have built-in modules of multichannel electrodes for cortex probing, deep brain stimulators, data processing chips, and wireless communication devices. For brain studies, it may also consist of an injection window and microfluidic sensors, as well as optical windows at multiple spots for long-time observation and optical experiments. The skull of a human adult has a large surface area; thus, it offers a large room for implantation of such a smart device.

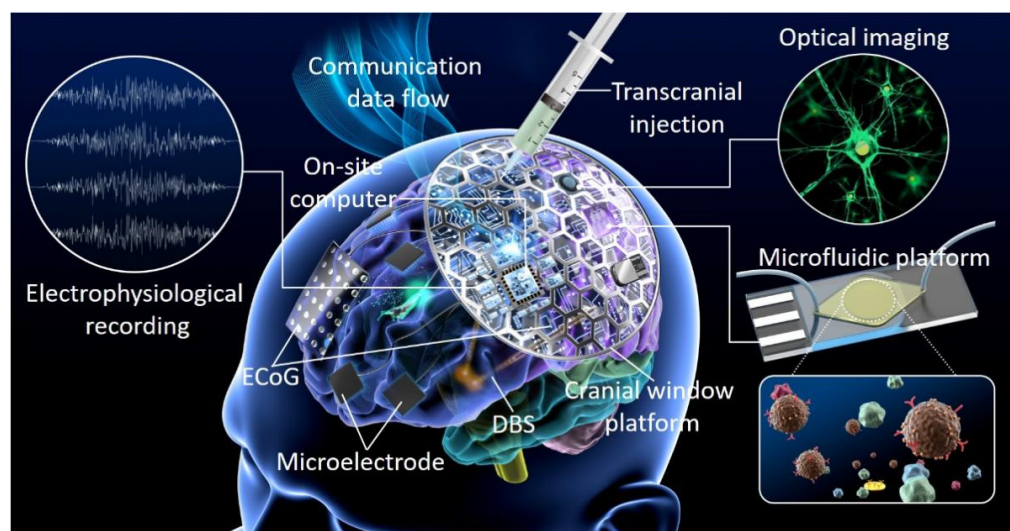


**Figure 6.** A proposal for a large-area multifunctional cranial window as a wearable smart electronic device for both medical and health care applications.

Such a smart cranial device may be applied in clinical surgery, such as treatment for cerebral apoplexy, repairing damage in brain tissue or skull bone from car accidents or shootings, removing cerebral hemorrhage, etc. It may also be used in treatment for chronic diseases, such as injecting drugs for inflammation and monitoring development for Alzheimer’s diseases or tumors.

## 5. Conclusions

In summary, in this paper we briefly reviewed developments of cranial windows, which offered a unique and direct approach for long-time direct observation of brain tissues and in vivo optical experiments with cortex neurons.

We presented preliminary results for our novel hybrid Ti-PDMS cranial windows. The Ti frames were made with 3D printing technique, and the PDMS layer was fixed on the frame with a multiple-stage process to ensure no remaining bubbles were in it. Experiments on mice and rats had shown excellent bio-compatibility of the device and excellent optical property for in vivo two-photon imaging and confocal imaging, as well as good self-sealing capability in multiple injections with commercial syringes. Tests showed that the 50 mm diameter, 1 mm thick honeycomb structured Ti frames had mechanical strength comparable to that of a human skull bone, meanwhile it had a large transparent area ratio of approximately 90%. Therefore, the Ti-PDMS hybrid devices have a promising potential for applications in brain studies in pigs, dogs, monkeys, and even humans as long-period, large-area, transparent and multifunctional cranial windows.

We also suggested that such a large-area multi-functional cranial window is indeed a good platform for a smart wearable electronic device implanted on the head that plays a key role in hybrid optical-electrical brain-computer interface in brain studies and serves as a drug delivery window for clinical applications. A smart cranial electronic device may have integrated modules for electrical probing, deep brain stimulation, data processing, and wireless communication, as well as a variety of on-site sensors, optical windows, and injection spots.

The results of this paper may shed light on the development of novel brain-computer interfaces and wearable electronic devices.

**Author Contributions:** Conceptualization, S.X., J.X., Q.L. and F.L.; methodology, Q.L., N.Y., J.X., S.X. and F.L.; validation, Q.L., F.L., N.Y. and X.Z.; formal analysis, N.Y., Q.L. and F.L.; investigation, N.Y., X.Z., Q.L. and F.L.; resources, Q.L., F.L. and S.X.; data curation, N.Y., X.Z., Q.L. and F.L.; writing—original draft preparation, N.Y., J.X. and S.X.; writing—review and editing, N.Y., Q.L., J.X. and F.L.; visualization, N.Y. and F.L.; supervision, F.L., Q.L. and S.X.; project administration, F.L., J.X. and S.X.; funding acquisition, F.L., Q.L. and S.X. All authors have read and agreed to the published version of the manuscript.

**Funding:** This work was funded by the National Key R&D Program of China, grant number 2017YFA0701302 (S.X., Q.L. and F.L.); the National Natural Science Foundation of China, grant numbers 32171002 (F.L.); and the Interdisciplinary Medicine Seed Fund of Peking University, grant number BMU2021MX002 (F.L.).

**Institutional Review Board Statement:** All animal experiments followed the guidelines of the Committee for Research and Ethical Issues of the International Association for the Study of Pain and were approved by the Animal Care and Use Committee of Peking University Health Science Center (LA2021571, approved on 21 November 2021).

**Data Availability Statement:** The data presented in this study are available on request from the corresponding author.

**Conflicts of Interest:** The authors declare no conflict of interest.

## References

1. Kennedy, D.; Norman, C. What don't we know? *Science* **2005**, *309*, 75. [[CrossRef](#)] [[PubMed](#)]
2. McGaugh, J.L. Memory—A century of consolidation. *Science* **2000**, *287*, 248–251. [[CrossRef](#)] [[PubMed](#)]
3. Todd, J.J.; Marois, R. Capacity limit of visual short-term memory in human posterior parietal cortex. *Nature* **2004**, *428*, 751–754. [[CrossRef](#)] [[PubMed](#)]
4. Park, H.J.; Friston, K. Structural and functional brain networks: From connections to cognition. *Science* **2013**, *342*, 1238411. [[CrossRef](#)]
5. Mizusaki, B.E.P.; Stepanyants, A.; Chklovskii, D.B.; Sjöström, P.J. Neocortex: A lean mean memory storage machine. *Nat. Neurosci.* **2016**, *19*, 643–644. [[CrossRef](#)]

6. Lodato, S.; Arlotta, P. Generating neuronal diversity in the mammalian cerebral cortex. *Annu. Rev. Cell Dev. Biol.* **2015**, *31*, 699–720. [[CrossRef](#)]
7. Fields, R. Neuroscience: Map the other brain. *Nature* **2013**, *501*, 25–27. [[CrossRef](#)]
8. Sunwoo, J.; Cornelius, N.R.; Doerschuk, P.C.; Schaffer, C.B. Estimating Brain Microvascular Blood Flows from Partial Two-Photon Microscopy Data by Computation with a Circuit Model. In Proceedings of the 2011 Annual International Conference of the IEEE Engineering in Medicine and Biology Society, Boston, MA, USA, 30 August–3 September 2011; pp. 174–177.
9. Shih, A.Y.; Driscoll, J.D.; Drew, P.J.; Nishimura, N.; Schaffer, C.B.; Kleinfeld, D. Two-photon microscopy as a tool to study blood flow and neurovascular coupling in the rodent brain. *J. Cereb. Blood Flow Metab.* **2012**, *32*, 1277–1309. [[CrossRef](#)]
10. Jessen, K. Glial cells. *Int. J. Biochem. Cell Biol.* **2004**, *36*, 1861–1867. [[CrossRef](#)]
11. Allen, N.J.; Lyons, D.A. Glia as architects of central nervous system formation and function. *Science* **2018**, *362*, 181–185. [[CrossRef](#)]
12. De Silva, T.M.; Faraci, F.M. Microvascular dysfunction and cognitive impairment. *Cell. Mol. Neurobiol.* **2016**, *36*, 241–258. [[CrossRef](#)] [[PubMed](#)]
13. Hosford, P.S.; Gourine, A.V. What is the key mediator of the neurovascular coupling response? *Neurosci. Biobehav. Rev.* **2019**, *96*, 174–181. [[CrossRef](#)] [[PubMed](#)]
14. Iadecola, C. The neurovascular unit coming of age: A journey through neurovascular coupling in health and disease. *Neuron* **2017**, *96*, 17–42. [[CrossRef](#)] [[PubMed](#)]
15. Miles, K.A. Brain perfusion: Computed tomography applications. *Neuroradiology* **2004**, *46*, S194–S200. [[CrossRef](#)] [[PubMed](#)]
16. Cook, C.K.L. Computed tomography of the brain: A pictorial review. *Hosp. Med.* **2004**, *65*, 8–12. [[CrossRef](#)]
17. Boto, E.; Holmes, N.; Leggett, J.; Roberts, G.; Shah, V.; Meyer, S.S.; Muñoz, L.D.; Mullinger, K.J.; Tierney, T.M.; Bestmann, S.; et al. Moving magnetoencephalography towards real-world applications with a wearable system. *Nature* **2018**, *555*, 657–661. [[CrossRef](#)] [[PubMed](#)]
18. Baillet, S. Magnetoencephalography for brain electrophysiology and imaging. *Nat. Neurosci.* **2017**, *20*, 327–339. [[CrossRef](#)] [[PubMed](#)]
19. Montagne, A.; Nation, D.A.; Sagare, A.P.; Barisano, G.; Sweeney, M.D.; Chakhoyan, A.; Pachicano, M.; Joe, E.; Nelson, A.R.; D’Orazio, L.M.; et al. APOE4 leads to blood–brain barrier dysfunction predicting cognitive decline. *Nature* **2020**, *581*, 71–76. [[CrossRef](#)]
20. Townsend, D.W. Positron emission tomography/computed tomography. *Semin. Nucl. Med.* **2008**, *38*, 152–166. [[CrossRef](#)]
21. Buckner, R.L.; Krienen, F.M.; Yeo, B.T.T. Opportunities and limitations of intrinsic functional connectivity MRI. *Nat. Neurosci.* **2013**, *16*, 832–837. [[CrossRef](#)]
22. Zuo, X.N.; Xing, X.X. Test-retest reliabilities of resting-state FMRI measurements in human brain functional connectomics: A systems neuroscience perspective. *Neurosci. Biobehav. Rev.* **2014**, *45*, 100–118. [[CrossRef](#)] [[PubMed](#)]
23. Ganesh, G.; Nakamura, K.; Saetia, S.; Tobar, A.M.; Yoshida, E.; Ando, H.; Yoshimura, N.; Koike, Y. Utilizing sensory prediction errors for movement intention decoding: A new methodology. *Sci. Adv.* **2018**, *4*, eaaq0183. [[CrossRef](#)] [[PubMed](#)]
24. Obidin, N.; Tasnim, F.; Dagdeviren, C. The future of neuroimplantable devices: A materials science and regulatory perspective. *Adv. Mater.* **2020**, *32*, 1901482. [[CrossRef](#)] [[PubMed](#)]
25. Luan, L.; Robinson, J.T.; Aazhang, B.; Chi, T.; Yang, K.; Li, X.; Rathore, H.; Singer, A.; Yellapantula, S.; Fan, Y.; et al. Recent advances in electrical neural interface engineering: Minimal invasiveness, longevity, and scalability. *Neuron* **2020**, *108*, 302–321. [[CrossRef](#)]
26. Hong, G.; Lieber, C. Novel electrode technologies for neural recordings. *Nat. Rev. Neurosci.* **2019**, *20*, 330–345. [[CrossRef](#)] [[PubMed](#)]
27. Hochberg, L.R.; Bacher, D.; Jarosiewicz, B.; Masse, N.Y.; Simeral, J.D.; Vogel, J.; Haddadin, S.; Liu, J.; Cash, S.S.; van der Smagt, P.; et al. Reach and grasp by people with tetraplegia using a neurally controlled robotic arm. *Nature* **2012**, *485*, 372–375. [[CrossRef](#)]
28. Ajiboye, A.B.; Willett, F.R.; Young, D.R.; Memberg, W.D.; Murphy, B.A.; Miller, J.P.; Walter, B.L.; Sweet, J.A.; Hoyen, H.A.; Keith, M.W.; et al. Restoration of reaching and grasping movements through brain-controlled muscle stimulation in a person with tetraplegia: A proof-of-concept demonstration. *Lancet* **2017**, *389*, 1821–1830. [[CrossRef](#)]
29. Brochier, T.; Zehl, L.; Hao, Y.; Duret, M.; Sprenger, J.; Denker, M.; Grün, S.; Riehle, A. Massively parallel recordings in macaque motor cortex during an instructed delayed reach-to-grasp task. *Sci. Data* **2018**, *5*, 180055. [[CrossRef](#)]
30. Chen, X.; Wang, F.; Fernandez, E.; Roelfsema, P.R. Shape perception via a high-channel-count neuroprosthesis in monkey visual cortex. *Science* **2020**, *370*, 1191–1196. [[CrossRef](#)]
31. Moses, D.A.; Leonard, M.K.; Makin, J.G.; Chang, E.F. Real-time decoding of question-and-answer speech dialogue using human cortical activity. *Nat. Commun.* **2019**, *10*, 3096–3110. [[CrossRef](#)]
32. Beauchamp, M.S.; Oswald, D.; Sun, P.; Foster, B.L.; Magnotti, J.F.; Niketeghad, S.; Pouratian, N.; Bosking, W.H.; Yoshor, D. Dynamic stimulation of visual cortex produces form vision in sighted and blind humans. *Cell* **2020**, *181*, 774–783.e775. [[CrossRef](#)] [[PubMed](#)]
33. Fekete, Z. Recent advances in silicon-based neural microelectrodes and microsystems: A review. *Sens. Actuators B Chem.* **2015**, *215*, 300–315. [[CrossRef](#)]
34. Vetter, R.J.; Williams, J.C.; Hetke, J.F.; Nunamaker, E.A.; Kipke, D.R. Chronic neural recording using silicon-substrate microelectrode arrays implanted in cerebral cortex. *IEEE Trans. Biomed. Eng.* **2004**, *51*, 896–904. [[CrossRef](#)] [[PubMed](#)]

35. Krauss, J.K.; Lipsman, N.; Aziz, T.; Boutet, A.; Brown, P.; Chang, J.W.; Davidson, B.; Grill, W.M.; Hariz, M.I.; Horn, A.; et al. Technology of deep brain stimulation: Current status and future directions. *Nat. Rev. Neurol.* **2021**, *17*, 75–87. [[CrossRef](#)] [[PubMed](#)]
36. Cramer, S.W.; Carter, R.E.; Aronson, J.D.; Kodandaramaiah, S.B.; Ebner, T.J.; Chen, C.C. Through the looking glass: A review of cranial window technology for optical access to the brain. *J. Neurosci. Methods* **2021**, *354*, 109100. [[CrossRef](#)] [[PubMed](#)]
37. Dunn, A.K.; Devor, A.; Bolay, H.; Andermann, M.L.; Moskowitz, M.A.; Dale, A.M.; Boas, D.A. Simultaneous imaging of total cerebral hemoglobin concentration, oxygenation, and blood flow during functional activation. *Opt. Lett.* **2003**, *28*, 28–30. [[CrossRef](#)] [[PubMed](#)]
38. Sun, X.; Wang, Y.; Chen, S.; Luo, W.; Li, P.; Luo, Q. Simultaneous monitoring of intracellular pH changes and hemodynamic response during cortical spreading depression by fluorescence-corrected multimodal optical imaging. *Neuroimage* **2011**, *57*, 873–884. [[CrossRef](#)]
39. Farkas, E.; Bari, F.; Obrenovitch, T.P. Multi-modal imaging of anoxic depolarization and hemodynamic changes induced by cardiac arrest in the rat cerebral cortex. *Neuroimage* **2010**, *51*, 734–742. [[CrossRef](#)]
40. Rickgauer, J.P.; Deisseroth, K.; Tank, D.W. Simultaneous cellular-resolution optical perturbation and imaging of place cell firing fields. *Nat. Neurosci.* **2014**, *17*, 1816–1824. [[CrossRef](#)]
41. Packer, A.M.; Russell, L.E.; Dalglish, H.W.P.; Häusser, M. Simultaneous all-optical manipulation and recording of neural circuit activity with cellular resolution in vivo. *Nat. Meth.* **2015**, *12*, 140–146. [[CrossRef](#)]
42. Ju, N.; Jiang, R.; Macknik, S.L.; Martinez-Conde, S.; Tang, S. Long-term all-optical interrogation of cortical neurons in awake-behaving nonhuman primates. *PLoS Biol.* **2018**, *16*, e2005839. [[CrossRef](#)] [[PubMed](#)]
43. Yang, W. Manipulating neuronal circuits, in concert. *Science* **2021**, *373*, 635. [[CrossRef](#)] [[PubMed](#)]
44. Guo, Z.V.; Li, N.; Huber, D.; Ophir, E.; Gutnisky, D.; Ting, J.T.; Feng, G.; Svoboda, K. Flow of cortical activity underlying a tactile decision in mice. *Neuron* **2014**, *81*, 179–194. [[CrossRef](#)] [[PubMed](#)]
45. Kim, T.H.; Zhang, Y.; Lecoq, J.; Jung, J.C.; Li, J.; Zeng, H.; Niell, C.M.; Schnitzer, M.J. Long-term optical access to an estimated one million neurons in the live mouse cortex. *Cell Rep.* **2016**, *17*, 3385–3394. [[CrossRef](#)] [[PubMed](#)]
46. Helmchen, F.; Denk, W. Deep tissue two-photon microscopy. *Nat. Meth.* **2005**, *2*, 932–940. [[CrossRef](#)]
47. Stosiek, C.; Garaschuk, O.; Holthoff, K.; Konnerth, A. In vivo two-photon calcium imaging of neuronal networks. *Proc. Natl. Acad. Sci. USA* **2003**, *100*, 7319. [[CrossRef](#)]
48. Baker, W.B.; Sun, Z.; Hiraki, T.; Putt, M.E.; Durduran, T.; Reivich, M.; Yodh, A.G.; Greenberg, J.H. Neurovascular coupling varies with level of global cerebral ischemia in a rat model. *J. Cereb. Blood Flow Metab.* **2012**, *33*, 97–105. [[CrossRef](#)]
49. Liu, Y.H.; Liao, L.D.; Tan, S.S.H.; Kwon, K.Y.; Ling, J.M.; Bandla, A.; Shih, Y.-Y.I.; Tan, E.T.W.; Li, W.; Ng, W.H.; et al. Assessment of neurovascular dynamics during transient ischemic attack by the novel integration of micro-electrocorticography electrode array with functional photoacoustic microscopy. *Neurobiol. Dis.* **2015**, *82*, 455–465. [[CrossRef](#)]
50. Luan, L.; Sullender, C.T.; Li, X.; Zhao, Z.; Zhu, H.; Wei, X.; Xie, C.; Dunn, A.K. Nanoelectronics enabled chronic multimodal neural platform in a mouse ischemic model. *J. Neurosci. Methods* **2018**, *295*, 68–76. [[CrossRef](#)]
51. Park, D.W.; Schendel, A.A.; Mikael, S.; Brodnick, S.K.; Richner, T.J.; Ness, J.P.; Hayat, M.R.; Atry, F.; Frye, S.T.; Pashaie, R.; et al. Graphene-based carbon-layered electrode array technology for neural imaging and optogenetic applications. *Nat. Commun.* **2014**, *5*, 5258–5269. [[CrossRef](#)]
52. Wang, B.; Zhou, J.; Carney, P.; Jiang, H. A novel detachable head-mounted device for simultaneous EEG and photoacoustic monitoring of epilepsy in freely moving rats. *Neurosci. Res.* **2015**, *91*, 57–62. [[CrossRef](#)] [[PubMed](#)]
53. Liao, L.D.; Liu, Y.H.; Lai, H.Y.; Bandla, A.; Shih, Y.Y.I.; Chen, Y.Y.; Thakor, N.V. Rescue of cortical neurovascular functions during the hyperacute phase of ischemia by peripheral sensory stimulation. *Neurobiol. Dis.* **2015**, *75*, 53–63. [[CrossRef](#)] [[PubMed](#)]
54. Zhao, C.; Li, D.; Guo, J.; Li, B.; Kong, Y.; Hu, Y.; Du, B.; Ding, Y.; Li, X.; Liu, H.; et al. The neurovascular couplings between electrophysiological and hemodynamic activities in anticipatory selective attention. *Cereb. Cortex* **2022**, bhab525. *Online ahead of print.* [[CrossRef](#)]
55. Kuzum, D.; Takano, H.; Shim, E.; Reed, J.C.; Juul, H.; Richardson, A.G.; de Vries, J.; Bink, H.; Dichter, M.A.; Lucas, T.H.; et al. Transparent and flexible low noise graphene electrodes for simultaneous electrophysiology and neuroimaging. *Nat. Commun.* **2014**, *5*, 5259. [[CrossRef](#)] [[PubMed](#)]
56. Luan, L.; Wei, X.; Zhao, Z.; Siegel, J.J.; Potnis, O.; Tuppen, C.A.; Lin, S.; Kazmi, S.; Fowler, R.A.; Holloway, S.; et al. Ultraflexible nanoelectronic probes form reliable, glial scar-free neural integration. *Sci. Adv.* **2017**, *3*, e1601966. [[CrossRef](#)] [[PubMed](#)]
57. Richner, T.J.; Thongpang, S.; Brodnick, S.K.; Schendel, A.A.; Falk, R.W.; Krugner-Higby, L.A.; Pashaie, R.; Williams, J.C. Optogenetic micro-electrocorticography for modulating and localizing cerebral cortex activity. *J. Neural Eng.* **2014**, *11*, 016010. [[CrossRef](#)]
58. Park, K.; You, J.; Du, C.; Pan, Y. Cranial window implantation on mouse cortex to study microvascular change induced by cocaine. *Quant. Imaging Med. Surg.* **2014**, *5*, 97–107. [[CrossRef](#)]
59. Park, D.W.; Brodnick, S.K.; Ness, J.P.; Atry, F.; Krugner-Higby, L.; Sandberg, A.; Mikael, S.; Richner, T.J.; Novello, J.; Kim, H.; et al. Fabrication and utility of a transparent graphene neural electrode array for electrophysiology, in vivo imaging, and optogenetics. *Nat. Protoc.* **2016**, *11*, 2201–2222. [[CrossRef](#)]
60. Zhang, J.; Liu, X.; Xu, W.; Luo, W.; Li, M.; Chu, F.; Xu, L.; Cao, A.; Guan, J.; Tang, S.; et al. Stretchable transparent electrode arrays for simultaneous electrical and optical interrogation of neural circuits in vivo. *Nano Lett.* **2018**, *18*, 2903–2911. [[CrossRef](#)]

61. Ghanbari, L.; Carter, R.E.; Rynes, M.L.; Dominguez, J.; Chen, G.; Naik, A.; Hu, J.; Sagar, M.A.K.; Haltom, L.; Mossazghi, N.; et al. Cortex-wide neural interfacing via transparent polymer skulls. *Nat. Commun.* **2019**, *10*, 1500–1513. [[CrossRef](#)]
62. Wang, X.; Wang, M.; Sheng, H.; Zhu, L.; Zhu, J.; Zhang, H.; Liu, Y.; Zhan, L.; Wang, X.; Zhang, J.; et al. Subdural neural interfaces for long-term electrical recording, optical microscopy and magnetic resonance imaging. *Biomaterials* **2022**, *281*, 121352. [[CrossRef](#)] [[PubMed](#)]
63. Yang, N.; Liu, F.; Zhang, X.; Chen, C.; Xia, Z.; Fu, S.; Wang, J.; Xu, J.; Cui, S.; Zhang, Y.; et al. A hybrid titanium-softmaterial, high-strength, transparent cranial window for transcranial injection and neuroimaging. *Biosensors* **2022**, *12*, 129. [[CrossRef](#)] [[PubMed](#)]
64. Roome, C.J.; Kuhn, B. Chronic cranial window with access port for repeated cellular manipulations, drug application, and electrophysiology. *Front. Cell. Neurosci.* **2014**, *8*, 379. [[CrossRef](#)] [[PubMed](#)]
65. Goldey, G.J.; Roumis, D.K.; Glickfeld, L.L.; Kerlin, A.M.; Reid, R.C.; Bonin, V.; Schafer, D.P.; Andermann, M.L. Removable cranial windows for long-term imaging in awake mice. *Nat. Protoc.* **2014**, *9*, 2515–2538. [[CrossRef](#)]
66. Tokuno, H.; Hatanaka, N.; Chiken, S.; Ishizuka, N. An improved method with a long-shanked glass micropipette and ultrasonography for drug injection into deep brain structure of the monkey. *Brain Res. Protoc.* **2002**, *10*, 16–22. [[CrossRef](#)]
67. Takehara, H.; Nagaoka, A.; Noguchi, J.; Akagi, T.; Kasai, H.; Ichiki, T. Lab-on-a-brain: Implantable micro-optical fluidic devices for neural cell analysis in vivo. *Sci. Rep.* **2014**, *4*, 6721. [[CrossRef](#)] [[PubMed](#)]
68. Vieira, D.B.; Gamarra, L.F. Getting into the brain: Liposome-based strategies for effective drug delivery across the blood-brain barrier. *Int. J. Nanomed.* **2016**, *11*, 5381–5414. [[CrossRef](#)]
69. Chen, W.; Zuo, H.; Zhang, E.; Li, L.; Henrich-Noack, P.; Cooper, H.; Qian, Y.; Xu, Z.P. Brain targeting delivery facilitated by ligand-functionalized layered double hydroxide nanoparticles. *ACS Appl. Mater. Interfaces* **2018**, *10*, 20326–20333. [[CrossRef](#)]
70. Liang, J.; Gao, C.; Zhu, Y.; Ling, C.; Wang, Q.; Huang, Y.; Qin, J.; Wang, J.; Lu, W.; Wang, J. Natural brain penetration enhancer-modified albumin nanoparticles for glioma targeting delivery. *ACS Appl. Mater. Interfaces* **2018**, *10*, 30201–30213. [[CrossRef](#)]
71. Gernert, M.; Feja, M. Bypassing the blood-brain barrier: Direct intracranial drug delivery in epilepsies. *Pharmaceutics* **2020**, *12*, 1134. [[CrossRef](#)]
72. Han, H.; Xia, Z.; Chen, H.; Hou, C.; Li, W. Simple diffusion delivery via brain interstitial route for the treatment of cerebral ischemia. *Sci. China Life Sci.* **2011**, *54*, 235–239. [[CrossRef](#)] [[PubMed](#)]
73. Park, J.; Jin, K.; Sahasrabudhe, A.; Chiang, P.-H.; Maalouf, J.H.; Koehler, F.; Rosenfeld, D.; Rao, S.; Tanaka, T.; Khudiyev, T.; et al. In situ electrochemical generation of nitric oxide for neuronal modulation. *Nat. Nanotechnol.* **2020**, *15*, 690–697. [[CrossRef](#)] [[PubMed](#)]
74. Heo, C.; Park, H.; Kim, Y.T.; Baeg, E.; Kim, Y.H.; Kim, S.G.; Suh, M. A soft, transparent, freely accessible cranial window for chronic imaging and electrophysiology. *Sci. Rep.* **2016**, *6*, 27818. [[CrossRef](#)] [[PubMed](#)]
75. Kunori, N.; Takashima, I. An implantable cranial window using a collagen membrane for chronic voltage-sensitive dye imaging. *Micromachines* **2019**, *10*, 789. [[CrossRef](#)]
76. Wang, Y.; Liang, G.; Liu, F.; Chen, Q.; Xi, L. A long-term cranial window for high-resolution photoacoustic imaging. *IEEE Trans. Biomed. Eng.* **2021**, *68*, 706–711. [[CrossRef](#)]
77. Donders, F. De bewegingen der hersenen en de veranderingen der vaatvulling van de pia mater, ook bij gesloten onuitzetbaren schedel regtstreeks onderzocht. *Ned. Lancet* **1850**, *5*, 521–553.
78. Donders, F.C. *Physiologie des Menschen*; S. Hirzel Verlag: Hirzel, Germany, 1859.
79. Forbes, H.S. The cerebral circulation: Observation and measurement of pial vessels. *Arch. Neurol. Psychiatry* **1928**, *19*, 751–761. [[CrossRef](#)]
80. Leyden, E. Beiträge und untersuchungen zur physiologie und pathologie des gehirns. *Arch. Pathol. Anat. Physiol. Klin. Med.* **1866**, *37*, 519–559. [[CrossRef](#)]
81. Cushing, H. Some experimental and clinical observations concerning states of increased intracranial tension. *Am. J. Med. Sci.* **1902**, *124*, 375. [[CrossRef](#)]
82. Lee, F.C. The effect of histamine on cerebrospinal fluid pressure. *Am. J. Physiol.-Leg. Content* **1925**, *74*, 317–325. [[CrossRef](#)]
83. Yang, G.; Pan, F.; Parkhurst, C.N.; Grutzendler, J.; Gan, W.B. Thinned-skull cranial window technique for long-term imaging of the cortex in live mice. *Nat. Protoc.* **2010**, *5*, 201–208. [[CrossRef](#)] [[PubMed](#)]
84. Christie, R.H.; Bacskai, B.J.; Zipfel, W.R.; Williams, R.M.; Kajdasz, S.T.; Webb, W.W.; Hyman, B.T. Growth arrest of individual senile plaques in a model of Alzheimer’s disease observed by in vivo multiphoton microscopy. *J. Neurosci.* **2001**, *21*, 858–864. [[CrossRef](#)] [[PubMed](#)]
85. Jeong, D.C.; Tsai, P.S.; Kleinfeld, D. All-optical osteotomy to create windows for transcranial imaging in mice. *Opt. Express* **2013**, *21*, 23160–23168. [[CrossRef](#)]
86. Nimmerjahn, A.; Kirchhoff, F.; Helmchen, F. Resting microglial cells are highly dynamic surveillants of brain parenchyma in vivo. *Science* **2005**, *308*, 1314–1318. [[CrossRef](#)] [[PubMed](#)]
87. Kim, J.V.; Kang, S.S.; Dustin, M.L.; McGavern, D.B. Myelomonocytic cell recruitment causes fatal CNS vascular injury during acute viral meningitis. *Nature* **2009**, *457*, 191–195. [[CrossRef](#)] [[PubMed](#)]
88. Tsai, J.; Grutzendler, J.; Duff, K.; Gan, W.B. Fibrillar amyloid deposition leads to local synaptic abnormalities and breakage of neuronal branches. *Nat. Neurosci.* **2004**, *7*, 1181–1183. [[CrossRef](#)] [[PubMed](#)]
89. Zuo, Y.; Lin, A.; Chang, P.; Gan, W.B. Development of long-term dendritic spine stability in diverse regions of cerebral cortex. *Neuron* **2005**, *46*, 181–189. [[CrossRef](#)]

90. Zuo, Y.; Yang, G.; Kwon, E.; Gan, W.B. Long-term sensory deprivation prevents dendritic spine loss in primary somatosensory cortex. *Nature* **2005**, *436*, 261–265. [[CrossRef](#)]
91. Grutzendler, J.; Kasthuri, N.; Gan, W.B. Long-term dendritic spine stability in the adult cortex. *Nature* **2002**, *420*, 812–816. [[CrossRef](#)]
92. Holtmaat, A.; Bonhoeffer, T.; Chow, D.K.; Chuckowree, J.; De Paola, V.; Hofer, S.B.; Hübener, M.; Keck, T.; Knott, G.; Lee, W.-C.A.; et al. Long-term, high-resolution imaging in the mouse neocortex through a chronic cranial window. *Nat. Protoc.* **2009**, *4*, 1128–1144. [[CrossRef](#)]
93. Drew, P.J.; Shih, A.Y.; Driscoll, J.D.; Knutsen, P.M.; Blinder, P.; Davalos, D.; Akassoglou, K.; Tsai, P.S.; Kleinfeld, D. Chronic optical access through a polished and reinforced thinned skull. *Nat. Meth.* **2010**, *7*, 981–984. [[CrossRef](#)] [[PubMed](#)]
94. Helm, P.J.; Ottersen, O.P.; Nase, G. Analysis of optical properties of the mouse cranium—Implications for in vivo multi photon laser scanning microscopy. *J. Neurosci. Methods* **2009**, *178*, 316–322. [[CrossRef](#)] [[PubMed](#)]
95. Tohmi, M.; Kitaura, H.; Komagata, S.; Kudoh, M.; Shibuki, K. Enduring critical period plasticity visualized by transcranial flavoprotein imaging in mouse primary visual cortex. *J. Neurosci.* **2006**, *26*, 11775–11785. [[CrossRef](#)] [[PubMed](#)]
96. Hira, R.; Honkura, N.; Noguchi, J.; Maruyama, Y.; Augustine, G.J.; Kasai, H.; Matsuzaki, M. Transcranial optogenetic stimulation for functional mapping of the motor cortex. *J. Neurosci. Methods* **2009**, *179*, 258–263. [[CrossRef](#)]
97. Wang, J.; Zhang, Y.; Xu, T.H.; Luo, Q.M.; Zhu, D. An innovative transparent cranial window based on skull optical clearing. *Laser Phys. Lett.* **2012**, *9*, 469–473. [[CrossRef](#)]
98. Zhang, C.; Zhao, Y.; Shi, R.; Zhu, D. A Rapid and Reversible Skull Optical Clearing Method for Monitoring Cortical Blood Flow. In *Dynamics and Fluctuations in Biomedical Photonics XIII*; SPIE BiOS: San Francisco, CA, USA, 2016; Volume 9707, p. 970717.
99. Yang, X.; Zhang, Y.; Zhao, K.; Zhao, Y.; Liu, Y.; Gong, H.; Luo, Q.; Zhu, D. Skull optical clearing solution for enhancing ultrasonic and photoacoustic imaging. *IEEE Trans. Med. Imaging* **2016**, *35*, 1903–1906. [[CrossRef](#)]
100. Zhao, Y.; Yu, T.; Zhang, C.; Li, Z.; Luo, Q.; Xu, T.H.; Zhu, D. Skull optical clearing window for in vivo imaging of the mouse cortex at synaptic resolution. *Light Sci. Appl.* **2018**, *7*, 17153. [[CrossRef](#)]
101. Zhang, C.; Feng, W.; Zhao, Y.; Yu, T.; Li, P.; Xu, T.; Luo, Q.; Zhu, D. A large, switchable optical clearing skull window for cerebrovascular imaging. *Theranostics* **2018**, *8*, 2696–2708. [[CrossRef](#)]
102. Li, D.Y.; Zheng, Z.; Yu, T.T.; Tang, B.Z.; Fei, P.; Qian, J.; Zhu, D. Visible-near infrared-II skull optical clearing window for in vivo cortical vasculature imaging and targeted manipulation. *J. Biophotonics* **2020**, *13*, e202000142. [[CrossRef](#)]
103. Zhang, C.; Feng, W. Assessment of tissue-specific changes in structure and function induced by in vivo skin/skull optical clearing techniques. *Lasers Surg. Med.* **2021**, *54*, 447–458. [[CrossRef](#)]
104. Svoboda, K.; Denk, W.; Kleinfeld, D.; Tank, D.W. In vivo dendritic calcium dynamics in neocortical pyramidal neurons. *Nature* **1997**, *385*, 161–165. [[CrossRef](#)] [[PubMed](#)]
105. Lendvai, B.; Stern, E.A.; Chen, B.; Svoboda, K. Experience-dependent plasticity of dendritic spines in the developing rat barrel cortex in vivo. *Nature* **2000**, *404*, 876–881. [[CrossRef](#)] [[PubMed](#)]
106. Trachtenberg, J.T.; Chen, B.E.; Knott, G.W.; Feng, G.; Sanes, J.R.; Welker, E.; Svoboda, K. Long-term in vivo imaging of experience-dependent synaptic plasticity in adult cortex. *Nature* **2002**, *420*, 788–794. [[CrossRef](#)] [[PubMed](#)]
107. Portera-Cailliau, C.; Weimer, R.M.; De Paola, V.; Caroni, P.; Svoboda, K. Diverse modes of axon elaboration in the developing neocortex. *PLoS Biol.* **2005**, *3*, e272. [[CrossRef](#)] [[PubMed](#)]
108. De Paola, V.; Holtmaat, A.; Knott, G.; Song, S.; Wilbrecht, L.; Caroni, P.; Svoboda, K. Cell type-specific structural plasticity of axonal branches and boutons in the adult neocortex. *Neuron* **2006**, *49*, 861–875. [[CrossRef](#)] [[PubMed](#)]
109. Lee, W.C.; Huang, H.; Feng, G.; Sanes, J.R.; Brown, E.N.; So, P.T.; Nedivi, E. Dynamic remodeling of dendritic arbors in GABAergic interneurons of adult visual cortex. *PLoS Biol.* **2006**, *4*, e29. [[CrossRef](#)]
110. Holtmaat, A.; de Paola, V.; Wilbrecht, L.; Trachtenberg, J.T.; Svoboda, K.; Portera-Cailliau, C. Imaging neocortical neurons through a chronic cranial window. *Cold Spring Harb. Protoc.* **2012**, *2012*, 694–701. [[CrossRef](#)]
111. Brown, C.E.; Aminoltejeri, K.; Erb, H.; Winship, I.R.; Murphy, T.H. In vivo voltage-sensitive dye imaging in adult mice reveals that somatosensory maps lost to stroke are replaced over weeks by new structural and functional circuits with prolonged modes of activation within both the peri-infarct zone and distant sites. *J. Neurosci.* **2009**, *29*, 1719–1734. [[CrossRef](#)]
112. Keck, T.; Mrcsic-Flogel, T.D.; Vaz Afonso, M.; Eysel, U.T.; Bonhoeffer, T.; Hübener, M. Massive restructuring of neuronal circuits during functional reorganization of adult visual cortex. *Nat. Neurosci.* **2008**, *11*, 1162–1167. [[CrossRef](#)]
113. O'Connor, D.H.; Peron, S.P.; Huber, D.; Svoboda, K. Neural activity in barrel cortex underlying vibrissa-based object localization in mice. *Neuron* **2010**, *67*, 1048–1061. [[CrossRef](#)]
114. Kobat, D.; Horton, N.; Xu, C. In vivo two-photon microscopy to 1.6-mm depth in mouse cortex. *J. Biomed. Opt.* **2011**, *16*, 106014. [[CrossRef](#)] [[PubMed](#)]
115. Horton, N.G.; Wang, K.; Kobat, D.; Clark, C.G.; Wise, F.W.; Schaffer, C.B.; Xu, C. In vivo three-photon microscopy of subcortical structures within an intact mouse brain. *Nat. Photonics* **2013**, *7*, 205–209. [[CrossRef](#)] [[PubMed](#)]
116. Santos, A.F.; Hübener, M. Chronic calcium imaging of neurons in the mouse visual cortex using a troponin C-based indicator. *Cold Spring Harb. Protoc.* **2014**, *2014*, 544–551. [[CrossRef](#)] [[PubMed](#)]
117. Choi, W.J.; Wang, R.K. Swept-source optical coherence tomography powered by a 1.3- $\mu\text{m}$  vertical cavity surface emitting laser enables 2.3-mm-deep brain imaging in mice in vivo. *J. Biomed. Opt.* **2015**, *20*, 106004. [[CrossRef](#)]

118. Dombeck, D.; Tank, D. Two-photon imaging of neural activity in awake mobile mice. *Cold Spring Harb. Protoc.* **2014**, *2014*, 726–736. [[CrossRef](#)]
119. Koletar, M.M.; Dorr, A.; Brown, M.E.; McLaurin, J.; Stefanovic, B. Refinement of a chronic cranial window implant in the rat for longitudinal in vivo two-photon fluorescence microscopy of neurovascular function. *Sci. Rep.* **2019**, *9*, 5499. [[CrossRef](#)]
120. Scott, B.B.; Thiberge, S.Y.; Guo, C.; Tervo, D.G.R.; Brody, C.D.; Karpova, A.Y.; Tank, D.W. Imaging cortical dynamics in GCaMP transgenic rats with a head-mounted widefield macroscope. *Neuron* **2018**, *100*, 1045–1058. [[CrossRef](#)]
121. Klein, S.P.; De Sloovere, V.; Meyfroidt, G.; Depreitere, B. Autoregulation assessment by direct visualisation of pial arterial blood flow in the piglet brain. *Sci. Rep.* **2019**, *9*, 13333. [[CrossRef](#)]
122. Smith, G.B.; Hein, B.; Whitney, D.E.; Fitzpatrick, D.; Kaschube, M. Distributed network interactions and their emergence in developing neocortex. *Nat. Neurosci.* **2018**, *21*, 1600–1608. [[CrossRef](#)]
123. Stettler, D.D.; Yamahachi, H.; Li, W.; Denk, W.; Gilbert, C.D. Axons and synaptic boutons are highly dynamic in adult visual cortex. *Neuron* **2006**, *49*, 877–887. [[CrossRef](#)]
124. Orringer, D.A.; Chen, T.; Huang, D.L.; Armstead, W.M.; Hoff, B.A.; Koo, Y.E.; Keep, R.F.; Philbert, M.A.; Kopelman, R.; Sagher, O. The brain tumor window model: A combined cranial window and implanted glioma model for evaluating intraoperative contrast agents. *Neurosurgery* **2010**, *66*, 736–743. [[CrossRef](#)] [[PubMed](#)]
125. Sunil, S.; Erdener, S.E.; Lee, B.S.; Postnov, D.; Tang, J.; Kura, S.; Cheng, X.; Chen, I.A.; Boas, D.A.; Kılıç, K. Awake chronic mouse model of targeted pial vessel occlusion via photothrombosis. *Neurophotonics* **2020**, *7*, 015005. [[CrossRef](#)] [[PubMed](#)]
126. Kauvar, I.V.; Machado, T.A.; Yuen, E.; Kochalka, J.; Choi, M.; Allen, W.E.; Wetzstein, G.; Deisseroth, K. Cortical observation by synchronous multifocal optical sampling reveals widespread population encoding of actions. *Neuron* **2020**, *107*, 351–367. [[CrossRef](#)] [[PubMed](#)]
127. Andermann, M.L.; Gilfoy, N.B.; Goldey, G.J.; Sachdev, R.N.; Wölfel, M.; McCormick, D.A.; Reid, R.C.; Levene, M.J. Chronic cellular imaging of entire cortical columns in awake mice using microprisms. *Neuron* **2013**, *80*, 900–913. [[CrossRef](#)]
128. Low, R.J.; Gu, Y.; Tank, D.W. Cellular resolution optical access to brain regions in fissures: Imaging medial prefrontal cortex and grid cells in entorhinal cortex. *Proc. Natl. Acad. Sci. USA* **2014**, *111*, 18739–18744. [[CrossRef](#)]
129. Beckmann, L.; Zhang, X.; Nadkarni, N.A.; Cai, Z.; Batra, A.; Sullivan, D.P.; Muller, W.A.; Sun, C.; Kuranov, R.; Zhang, H.F. Longitudinal deep-brain imaging in mouse using visible-light optical coherence tomography through chronic microprism cranial window. *Biomed. Opt. Express* **2019**, *10*, 5235–5250. [[CrossRef](#)]
130. Levene, M.J.; Dombeck, D.A.; Kasischke, K.A.; Molloy, R.P.; Webb, W.W. In vivo multiphoton microscopy of deep brain tissue. *J. Neurophysiol.* **2004**, *91*, 1908–1912. [[CrossRef](#)]
131. Bocarsly, M.E.; Jiang, W.C.; Wang, C.; Dudman, J.T.; Ji, N.; Aponte, Y. Minimally invasive microendoscopy system for in vivo functional imaging of deep nuclei in the mouse brain. *Biomed. Opt. Express* **2015**, *6*, 4546–4556. [[CrossRef](#)]
132. Pernici, C.D.; Rowe, R.K.; Doughty, P.T.; Madadi, M.; Lifshitz, J.; Murray, T.A. Longitudinal optical imaging technique to visualize progressive axonal damage after brain injury in mice reveals responses to different minocycline treatments. *Sci. Rep.* **2020**, *10*, 7815. [[CrossRef](#)]
133. Sato, M.; Sano, S.; Watanabe, H.; Kudo, Y.; Nakai, J. An aspherical microlens assembly for deep brain fluorescence microendoscopy. *Biochem. Biophys. Res. Commun.* **2020**, *527*, 447–452. [[CrossRef](#)]
134. Park, H.; You, N.; Lee, J.; Suh, M. Longitudinal study of hemodynamics and dendritic membrane potential changes in the mouse cortex following a soft cranial window installation. *Neurophotonics* **2019**, *6*, 015006. [[CrossRef](#)] [[PubMed](#)]
135. Rosenthal, Z.P.; Raut, R.V.; Yan, P.; Koko, D.; Kraft, A.W.; Czerniewski, L.; Acland, B.; Mitra, A.; Snyder, L.H.; Bauer, A.Q.; et al. Local perturbations of cortical excitability propagate differentially through large-scale functional networks. *Cereb. Cortex* **2020**, *30*, 3352–3369. [[CrossRef](#)] [[PubMed](#)]
136. Miao, P.; Zhang, L.; Li, M.; Zhang, Y.; Feng, S.; Wang, Q.; Thakor, N.V. Chronic wide-field imaging of brain hemodynamics in behaving animals. *Biomed. Opt. Express* **2017**, *8*, 436–445. [[CrossRef](#)] [[PubMed](#)]
137. Thunemann, M.; Lu, Y.; Liu, X.; Kılıç, K.; Desjardins, M.; Vandenberghe, M.; Sadegh, S.; Saisan, P.A.; Cheng, Q.; Weldy, K.L.; et al. Deep 2-photon imaging and artifact-free optogenetics through transparent graphene microelectrode arrays. *Nat. Commun.* **2018**, *9*, 2035–2047. [[CrossRef](#)]
138. Kozai, T.D.Y.; Vazquez, A.L. Photoelectric artefact from optogenetics and imaging on microelectrodes and bioelectronics: New challenges and opportunities. *J. Mater. Chem. B* **2015**, *3*, 4965–4978. [[CrossRef](#)] [[PubMed](#)]
139. Benfenati, V.; Toffanin, S.; Bonetti, S.; Turatti, G.; Pistone, A.; Chiappalone, M.; Sagnella, A.; Stefani, A.; Generali, G.; Ruani, G.; et al. A transparent organic transistor structure for bidirectional stimulation and recording of primary neurons. *Nat. Mater.* **2013**, *12*, 672–680. [[CrossRef](#)]
140. Lee, W.; Kim, D.; Matsuhisa, N.; Nagase, M.; Sekino, M.; Malliaras, G.G.; Yokota, T.; Someya, T. Transparent, conformable, active multielectrode array using organic electrochemical transistors. *Proc. Natl. Acad. Sci. USA* **2017**, *114*, 10554–10559. [[CrossRef](#)]
141. Rengier, F.; Mehndiratta, A.; von Tengg-Kobligk, H.; Zechmann, C.M.; Unterhinninghofen, R.; Kauczor, H.U.; Giesel, F.L. 3D printing based on imaging data: Review of medical applications. *Int. J. Comput. Assist. Radiol. Surg.* **2010**, *5*, 335–341. [[CrossRef](#)]
142. Naftulin, J.S.; Kimchi, E.Y.; Cash, S.S. Streamlined, inexpensive 3D printing of the brain and skull. *PLoS ONE* **2015**, *10*, e0136198. [[CrossRef](#)]
143. Zhou, L.Y.; Fu, J.; He, Y. A review of 3D printing technologies for soft polymer materials. *Adv. Funct. Mater.* **2020**, *30*, 2000187. [[CrossRef](#)]

144. Li, J.; Pumera, M. 3D printing of functional microrobots. *Chem. Soc. Rev.* **2021**, *50*, 2794–2838. [[CrossRef](#)] [[PubMed](#)]
145. Ma, I.T.; Symon, M.R.; Bristol, R.E.; Beals, S.P.; Joganic, E.F.; Adelson, P.D.; Shafron, D.H.; Singh, D.J. Outcomes of titanium mesh cranioplasty in pediatric patients. *J. Craniofac. Surg.* **2018**, *29*, 99–104. [[CrossRef](#)] [[PubMed](#)]
146. Luo, J.; Liu, B.; Xie, Z.; Ding, S.; Zhuang, Z.; Lin, L.; Guo, Y.; Chen, H.; Yu, X. Comparison of manually shaped and computer-shaped titanium mesh for repairing large frontotemporoparietal skull defects after traumatic brain injury. *Neurosurg. Focus* **2012**, *33*, e13. [[CrossRef](#)]
147. Lam, S.; Kuether, J.; Fong, A.; Reid, R. Cranioplasty for large-sized calvarial defects in the pediatric population: A review. *Craniofac. Trauma Reconstr.* **2015**, *8*, 159–170. [[CrossRef](#)]
148. Goldstein, J.A.; Paliga, J.T.; Bartlett, S.P. Cranioplasty: Indications and advances. *Curr. Opin. Otolaryngol. Head Neck Surg.* **2013**, *21*, 400–409. [[CrossRef](#)]
149. Zhu, S.; Chen, Y.; Lin, F.; Chen, Z.; Jiang, X.; Zhang, J.; Wang, J. Complications following titanium cranioplasty compared with nontitanium implants cranioplasty: A systematic review and meta-analysis. *J. Clin. Neurosci.* **2021**, *84*, 66–74. [[CrossRef](#)]
150. Lewitz, M.; Salma, A.; Welzel Saravia, H.; Sakellaropoulou, I.; Sarkis, H.M.; Ewelt, C.; Fortmann, T.; Wilbers, E.; Schipmann, S.; Suero Molina, E.; et al. Load-bearing capacity and design advantages of a custom-made, thin pure-titanium cranioplasty (craniotop). *J. Craniofac. Surg.* **2021**, *32*, 1291–1296. [[CrossRef](#)]
151. Maher, S.; Kaur, G.; Lima-Marques, L.; Evdokiou, A.; Losic, D. Engineering of micro- to nanostructured 3D-printed drug-releasing titanium implants for enhanced osseointegration and localized delivery of anticancer drugs. *ACS Appl. Mater. Interfaces* **2017**, *9*, 29562–29570. [[CrossRef](#)] [[PubMed](#)]
152. Qi, C.; Jiang, F.; Yang, S. Advanced honeycomb designs for improving mechanical properties: A review. *Compos. B. Eng.* **2021**, *227*, 109393. [[CrossRef](#)]
153. Zhang, J.; Lu, G.; You, Z. Large deformation and energy absorption of additively manufactured auxetic materials and structures: A review. *Compos. B. Eng.* **2020**, *201*, 108340. [[CrossRef](#)]
154. Wang, Q.; Li, Z.; Zhang, Y.; Cui, S.; Yang, Z.; Lu, Z. Ultra-low density architected metamaterial with superior mechanical properties and energy absorption capability. *Compos. B. Eng.* **2020**, *202*, 108379. [[CrossRef](#)]
155. Chen, S.; Tan, X.; Hu, J.; Zhu, S.; Wang, B.; Wang, L.; Jin, Y.; Wu, L. A novel gradient negative stiffness honeycomb for recoverable energy absorption. *Compos. B. Eng.* **2021**, *215*, 108745. [[CrossRef](#)]
156. Hales, T.C. The honeycomb conjecture. *Discret. Comput. Geom.* **2001**, *25*, 1–22. [[CrossRef](#)]
157. Zhang, Q.; Yang, X.; Li, P.; Huang, G.; Feng, S.; Shen, C.; Han, B.; Zhang, X.; Jin, F.; Xu, F.; et al. Bioinspired engineering of honeycomb structure -using nature to inspire human innovation. *Prog. Mater. Sci.* **2015**, *74*, 332–400. [[CrossRef](#)]
158. Torimitsu, S.; Nishida, Y.; Takano, T.; Yajima, D.; Inokuchi, G.; Makino, Y.; Motomura, A.; Chiba, F.; Yamaguchi, R.; Hashimoto, M.; et al. Differences in biomechanical properties and thickness among frontal and parietal bones in a Japanese sample. *Forensic Sci. Int.* **2015**, *252*, 191–196. [[CrossRef](#)] [[PubMed](#)]
159. Chen, L.M.; Heider, B.; Williams, G.V.; Healy, F.L.; Ramsden, B.M.; Roe, A.W. A chamber and artificial dura method for long-term optical imaging in the monkey. *J. Neurosci. Methods* **2002**, *113*, 41–49. [[CrossRef](#)]
160. Feng, P.; Wang, X.; Lu, B.; Pan, G.; Leng, X.; Ma, X.; Zhang, J.; Zhao, W. Ionic liquids-filled patterned cavities improve transmittance of transparent and stretchable electronic polydimethylsiloxane films. *J. Mater. Sci.* **2019**, *54*, 11134–11144. [[CrossRef](#)]
161. Guan, F.; Song, Z.; Xin, F.; Wang, H.; Yu, D.; Li, G.; Liu, W. Preparation of hydrophobic transparent paper via using polydimethylsiloxane as transparent agent. *J. Bioresour. Bioprod.* **2020**, *5*, 37–43. [[CrossRef](#)]
162. Świerczek-Lasek, B.; Keremidarska-Markova, M.; Hristova-Panusheva, K.; Vladkova, T.; Ciemerych, M.A.; Archacka, K.; Krasteva, N. Polydimethylsiloxane materials with supraphysiological elasticity enable differentiation of myogenic cells. *J. Biomed. Mater. Res. A* **2019**, *107*, 2619–2628. [[CrossRef](#)]
163. Shtoyerman, E.; Arieli, A.; Slovin, H.; Vanzetta, I.; Grinvald, A. Long-term optical imaging and spectroscopy reveal mechanisms underlying the intrinsic signal and stability of cortical maps in V1 of behaving monkeys. *J. Neurosci. Methods* **2000**, *20*, 8111–8121. [[CrossRef](#)]
164. Ryu, M.; Kim, J.; Lee, S.; Kim, J.; Song, T. Stretchable and transparent paper based on PDMS–CNC composite for direct printing. *Adv. Mater. Technol.* **2021**, *6*, 2100156. [[CrossRef](#)]
165. Musk, E. An integrated brain-machine interface platform with thousands of channels. *J. Med. Internet Res.* **2019**, *21*, e16194. [[CrossRef](#)] [[PubMed](#)]